Magnetic Properties of B-Rich Nano-Composite $RE_yTM_{90-y-x}Nb_xB_{10}$ Alloys

Israel Betancourt[1], Hywel A. Davies[2]

(1. Instituto de Investigaciones en Materiales, Universidad Nacional Autónoma de México. P.O. Box 70-360, Mexico D.F. 04510. Mexico; 2. Deparment of Engineering Materials, University of Sheffield, Mappin St., Sheffield S1 3JD, UK)

Abstract: We report and discuss the results of a study of the structures and magnetic properties of B-rich (10 at%) nanocomposite alloys, based on the formula $RE_yTM_{90-y-x}Nb_xB_{10}$ (RE=Nd, Nd+Pr, TM=Fe, Fe+Co; y=8,10,12, x=0,2,4) and processed by devitrification of melt-spun amorphous precursors. Considerable enhancement of the intrinsic coercivity, together with good to excellent remanence and energy density values were observed for Co-containing compositions with y =10 and x =2,4 . The intrinsic coercivity and remanence enhancements are ascribed to the grain refining effects of Nb, particularly with respect to the soft magnetic phases, and thus to more complete exchange coupling of the soft grains to the hard phase grains than for the Nb-free alloy.

Key words: nanocomposite alloy; hard magnetic material; enhanced coercivity

1 Introduction

Nanocomposite exchange enhanced hard magnetic alloys have been intensively studied since their first experimental and theoretical description[1-3]. These alloys comprise a fine mixture of hard magnetic crystallites ($R_2Fe_{14}B$[2,3], $R_2Fe_{17}N_x$[4] or $R_2Fe_{17}C_x$[5], R=Nd or Pr) interspersed with soft magnetic grains (α-Fe[3-5] or Fe_3B[2]). The corresponding soft/hard mean grain sizes are predicted by numerical simulations [6] to be ideally of diameter 10 nm for the soft phase and 20 nm for the hard phase, in order to avoid independent magnetization reversal at the soft grains and, thus, promote optimum ferromagnetic exchange coupling between hard and soft magnetic phases. Such exchange interaction leads to enhanced values of remanence, J_r, to well above the Stoner-Wohlfarth value of 0.5 J_s, but with reduced intrinsic coercivity ${}_iH_c$ (usually within the range 250-500 kA/m, depending on composition). Furthermore, their reduced rare-earth content decreases the raw material cost, which represent a useful advantage for commercial purposes. For the melt spun alloys having intermediate RE concentrations (8-11 at%) and a stoichiometric B content of ~6 at%, produced by direct quenching from the liquid state, the high cooling rate during the rapid solidification facilitates very large undercoolings and very high nucleation frequencies for both $R_2Fe_{14}B$ and α-Fe crystallites. This yields very fine grained structures with optimum magnetic properties. However, a major practical impediment for the full exploitation of this class of nanocomposite alloy is the narrow process window and the tendency to produce a range of ribbon thicknesses in a batch and thus with variable microstructure and properties[7]. An alternative process route is to "overquench" the alloy to the fully amorphous state followed by a devitrification anneal. This has been shown to give broadly comparable microstructures and magnetic properties to those obtained by direct quenching for stoichiometric $R_2Fe_{14}B$ alloys[8,9]. However, for overquenched, initially amorphous RFeB alloys with Fe-rich compositions (R content < 11.7 at%), the microstructural evolution on annealing begins with the precipitation and growth of α-Fe grains[10-12] followed by the formation and growth of the $R_2Fe_{14}B$ crystallites. This process tends to result in undesirably coarse α-Fe crystallites, which leads to incomplete

exchange coupling to the hard phase grains and, thus, to inferior magnetic properties for the composite structure[10,13]. The addition of small concentrations of refractory elements (Zr or Nb) has been reported as useful for controlling the growth of the soft phase[14,15].

In addition, Co inclusion in these nanocomposite alloys has been extensively used for improving thermal stability through higher Curie temperatures [9,16] and, consequently, superior temperature coefficients for both J_r and ${}_iH_c$[17]. Recently, an excess content of B [18,19] and excess B plus Ti and C additions[20] has been reported as giving a marked improvement in ${}_iH_c$ for α-Fe/$R_2Fe_{14}B$ alloys having rare earth concentrations ≤ 10 at% . In the present paper, we report the effects of an excess concentration of B (10 at%), Nb additions (up to 4 at%) and Co replacement for Fe, on the microstructure and magnetic properties of stoichiometric single phase 2/14/1 ribbons and nanocomposite α-(Fe, Co)/$R_2(Fe,Co)_{14}B$ alloys with rare earth contents of 8 at% and 10 at% .

2 Experimental

Ingots of the alloys, having compositions $RE_yTM_{90-y-x}Nb_xB_{10}$ (RE=Nd, $Nd_{0.75}Pr_{0.25}$; TM= Fe, $Fe_{0.9}Co_{0.1}$; y=8, 10, 12; x=0, 2,4) were prepared using commercial grade materials by arc-melting the constituents in a high purity Ar atmosphere. Overquenched and annealed (OA) samples were obtained by a devitrification anneal (10 min at 700 °C with material sealed in a silica tube under argon) of initially fully amorphous alloy ribbon, produced by melt spinning at 30 m/s. The magnetic properties J_r, ${}_iH_c$ and the maximum energy product $(BH)_{max}$ were determined using an Oxford 'Maglab' vibrating sample magnetometer (VSM) system with a maximum field of 5 T. The microstructure of selected ribbon samples was monitored by x-ray diffraction (XRD) analysis with Cu-Kα radiation and by transmission electron microscopy (TEM).

3 Results and Discussion

3.1 Single phase stoichiometric alloys

X-ray diffractograms for $Nd_{12}Fe_{82}B_6$, $(Nd_{0.75}Pr_{0.25})_{12}Fe_{82}B_6$ and $(Nd_{0.75}Pr_{0.25})_{12}Fe_{78}B_{10}$ OA alloy ribons are shown in Fig. 1. All the peaks correspond to the hard magnetic $RE_2Fe_{14}B$ phase, which is in accord with previous results for melt spun alloys with 12% at RE content[21].

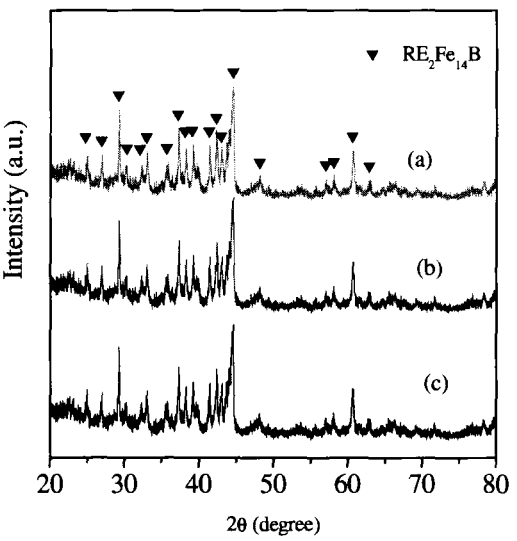

Fig. 1 X-ray diffractograms for stoichiometric $Nd_{12}Fe_{82}B_6$ (a), $(Nd_{0.75}Pr_{0.25})_{12}Fe_{82}B_6$ (b) and $(Nd_{0.75}Pr_{0.25})_{12}Fe_{78}B_{10}$ (c) OA alloy ribbons

Partial replacement of Nd by Pr results apparently in a slight increase in the proportion of the 2/14/1 phase [22], though the B enrichment seems not to affect the phase distribution at this RE concentration. The demagnetising quadrants of the *J-H* curves for all the alloys are displayed in Fig. 2.

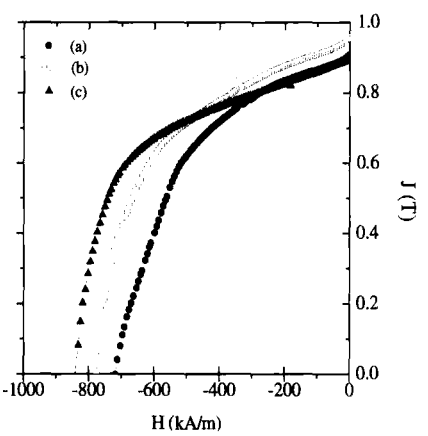

Fig. 2 Demagnetising curves for stoichiometric $Nd_{12}Fe_{82}B_6$ (a), $(Nd_{0.75}Pr_{0.25})_{12}Fe_{82}B_6$ (b) and $(Nd_{0.75}Pr_{0.25})_{12}Fe_{78}B_{10}$ (c) OA alloy ribbons

Enhanced J_r values (of ~ 0.9 T and above), compared with the expected value of 0.5 J_s for

uniaxial, single domain non-interacting particles, are evident for all the ribbons samples [21]. The energy densities are all >120 kJ/m^3 and, for the $(Nd_{0.75}Pr_{0.25})_{12}Fe_{82}B_6$ ribbon, it is in fact >145 kJ/m^3. The intrinsic coercivity undergoes a marked increase on partial replacement of Nd by Pr (792 kA/m compared with the original 713 kA/m for $Nd_{12}Fe_{82}B_6$) and a further enhancement up to 842 kA/m on increasing the B content to 10 at%. The properties are summarised in Table 1.

Table 1 Magnetic properties of stoichiometric OA alloy ribbons

Alloy composition	$_iH_c$ (kA/m)	J_r (T)	J_s (T)	$(BH)_{max}$ (kJ/m^3)
$Nd_{12}Fe_{82}B_6$	713∓7	0.91∓0.01	1.41∓0.02	120∓4
$(Nd_{0.75}Pr_{0.25})_{12}Fe_{82}B_6$	792∓15	0.98∓0.02	1.47∓0.02	146∓6
$(Nd_{0.75}Pr_{0.25})_{12}Fe_{78}B_{10}$	842∓10	0.91∓0.01	1.39∓0.02	129∓3

The observed remanence enhancement is a consequence of the inter-crystalline exchange coupling for a mean 2/14/1 grain size below 40 nm [21]. The good $(BH)_{max}$ values also result from good squareness of the curves, particularly for the Pr-containing alloys, which, in turn, are also indicative of a homogenous grain size distribution. However, the decrease in $(BH)_{max}$ between $(Nd_{0.75}Pr_{0.25})_{12}Fe_{82}B_6$ and $(Nd_{0.75}Pr_{0.25})_{12}Fe_{78}B_{10}$ probably reflects the fact that at least part of the soft phase in the latter is Fe_3B rather than α-Fe and that the Fe_3B has a lower J_s. The improvement achieved for $_iH_c$ can be attributed to a higher anisotropy field H_A associated with Pr substitution and, for the $(Nd_{0.75}Pr_{0.25})_{12}Fe_{78}B_{10}$ alloy, with the reduced J_r.

3.2 Nancomposite α -Fe/$RE_2Fe_{14}B$ alloys

Diffractograms for the OA $(Nd_{0.75}Pr_{0.25})_{10}Fe_{80-x}Nb_xB_{10}$(x=0, 2, 4) ribbon series are shown in Fig. 3. For the Nb-free alloy, the presence of bcc α-Fe phase is manifested as a strong diffraction peak at 2θ=44.6° (corresponding to the (110) reflection), together with peaks for the 2/14/1 hard phase. As the Nb content increases, the intensity of the α-Fe peak exhibits a progressive decrease, consistent with a decrease in volume fraction of this phase, and the peak breadth increases, reflecting also the effect of Nb as a grain size controller.

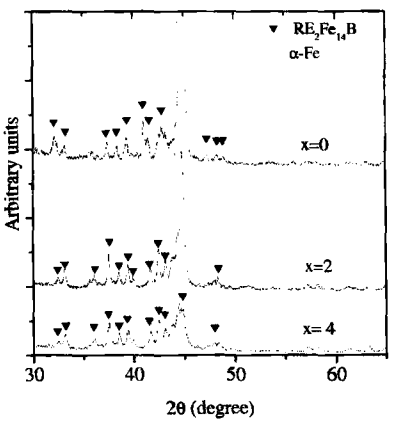

Fig. 3 X-ray diffractograms for the OA$(Nd_{0.75}Pr_{0.25})_{10}Fe_{80x}Nb_xB_{10}$ (x=0,2,4) alloy ribbon series

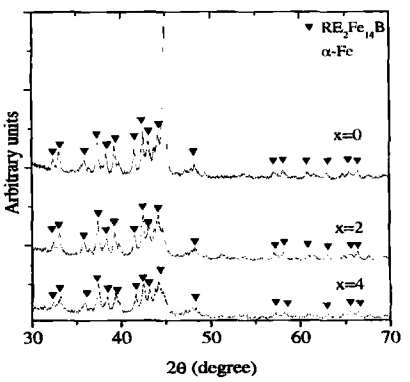

Fig. 4 X-ray diffractograms for the OA $(Nd_{0.75}Pr_{0.25})_8Fe_{82-x}Nb_xB_{10}$ (x=0,2,4) alloy ribbon series

Similar results were observed for the alloy series with RE=8 at% but with a much more pronounced initial (110) α -Fe reflection (Fig. 4), consistent with the higher Fe:RE ratio in this compositional series.

Transmission electron micrographs for two selected nanocomposite alloys, $RE_8Fe_{82}B_{10}$ and $RE_8Fe_{78}Nb_4B_{10}$, are shown in Fig. 5. For the Nb- free sample, Fig. 5 (a) shows a nanostructure comprised of smaller grains (< 15 nm, presumably hard 2/14/1 phase) and much larger crystallites (> 50 nm, evidently α-Fe, due to their dislocated internal structure), whilst for the alloy with 4 at% of Nb, Fig. 5(b), a homogeneous grain size distribution with mean grain diameters for both soft and hard phases of < 25

nm, confirming the grain size controlling effect of the Nb addition and presumably also the decreased volume fraction of soft phase.

The second quadrants of the *J-H* loops for the two alloy series $(Nd_{0.75}Pr_{0.25})_8Fe_{82-x}Nb_xB_{10}$(x=0, 2, 4) $(Nd_{0.75}Pr_{0.25})_{10}Fe_{80-x}Nb_xB_{10}$(x=0, 2, 4) are shown in Fig. 6 and Fig. 7, respectively. For the RE =8 at% series (Fig.6), $_iH_c$ increases progressively as the Nb concentration increases, from 228 kA/m (x=0) to 657 kA/m (x=4), though with a marked reduction in J_r. between 2 and 4 at% Nb. $(BH)_{max}$ is increased significantly on adding Nb, from 60 kJ/m^3 up to 117 kJ/m^3 for the 2 at% Nb alloy, with a slight drop on increasing to 4at%. The observed values of J_r and $_iH_c$ and the derived values of $(BH)_{max}$ for each composition are given in Table 2.

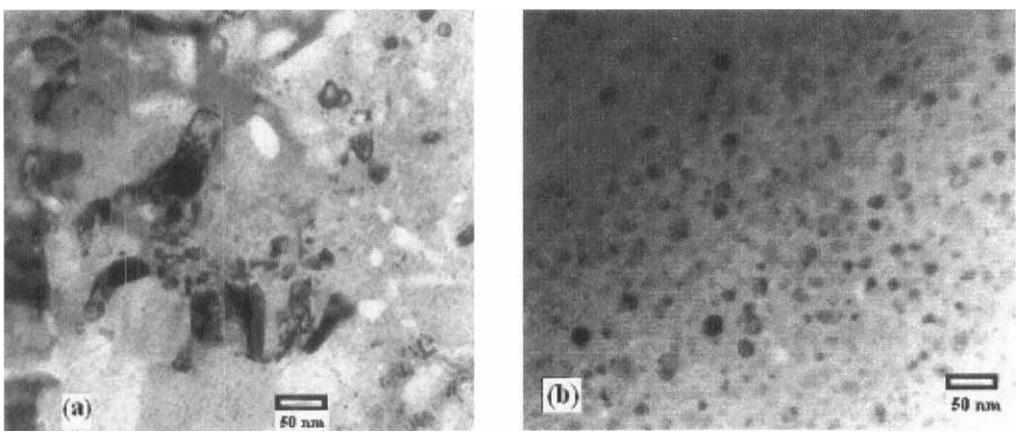

Fig. 5 TEM micrographs for nanocomposite OA $RE_8Fe_{82}B_{10}$ (a) and $RE_8Fe_{78}Nb_4B_{10}$ (b) ribbons

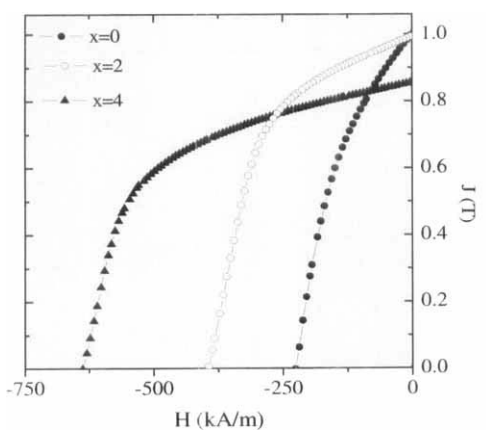

Fig. 6 J-H demagnetising curves for OA $(Nd_{0.75}Pr_{0.25})_8$-$Fe_{82-x}Nb_xB_{10}$ (x=0, 2, 4) alloy ribbon series

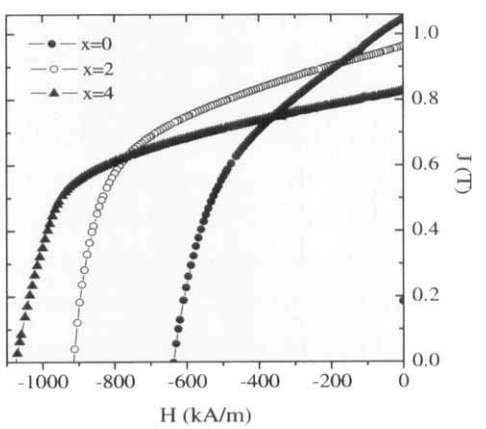

Fig. 7 J-H demagnetising curves for OA $(Nd_{0.75}Pr_{0.25})_{10}$-$Fe_{80-x}Nb_xB_{10}$ (x=0, 2, 4) alloy ribbon series

Table 2 Magnetic properties of OA ribbon samples of alloys in system $(Nd_{0.75}Pr_{0.25})_yFe_{90-y-x}Nb_xB_{10}$

RE content (y): Nb content (x)	$_iH_c$ (kA/m)	J_r (T)	J_s (T)	$(BH)_{max}$ (kJ/m^3)
y=8, x=0	228 ± 10	1.04 ± 0.06	1.75 ± 0.04	60 ± 7
y=8, x=2	420 ± 20	0.98 ± 0.04	1.56 ± 0.06	117 ± 5
y=8, x=4	657 ± 10	0.87 ± 0.01	1.31 ± 0.01	113 ± 2
y=10, x=0	619 ± 24	1.05 ± 0.02	1.60 ± 0.02	128 ± 9
y=10, x=2	912 ± 5	0.96 ± 0.01	1.47 ± 0.02	140 ± 6

For the RE=10 at% series (Fig.7), consistently larger $_iH_c$ values were observed, ranging from 619 kA/m for the Nb-free alloy to 1060 kA/m for the 4 at%Nb composition, reflecting the smaller volume fraction of soft magnetic phases present, and with $(BH)_{max}$ being as high as 140 kJ/m^3 for the 2 at% Nb alloy. Table 2 summarises these experimental data.

The substantial enhancement of $_iH_c$ and improved squareness of the loops on addition of up to 4 at% Nb

can be ascribed to its effects in promoting grain size refinement, notably of the soft phase, and narrowing of the grain size distribution. This effect has been described by micromagnetic simulations for nanocomposite α-Fe/$Nd_2Fe_{14}B$alloys[6,23]. According to these simulations, $_iH_c$ is predicted to increase with decreasing soft/hard mean grain sizes due to the enhanced inter-grain exchange interactions between the two phases. This is expected to suppress the nucleation of reverse domains within the soft grains, thus retarding the magnetization reversal of the neighbouring hard grains to higher applied fields and giving rise to improved $_iH_c$ values. A tendency for $_iH_c$ to increase with decreasing grain size was previously observed experimentally for Nb-free, intermediate $_iH_c$ (< 400 kA/m) nanocomposite α-Fe/$Nd_2Fe_{14}B$ alloys with a soft phase volume fraction of 30% [24]. The higher $_iH_c$ for the 10at% RE alloys than for the corresponding 8at% RE alloys is due to the consistently larger volume fraction of hard 2/14/1 phase in the former. The high J_r for the Nb-free compositions, especially for the 8 at% RE alloy, reflects the high J_s associated with a large volume fraction of α-Fe. However, J_s decreases rapidly with increasing Nb content, indicating that it enters the 2/14/1 unit cell and reduces the nett magnetic moment, and this has a corresponding effect on J_r. For each series, the highest $(BH)_{max}$ corresponds to 2 at% of Nb. Evidently, the effect of 2 at% Nb represents a good compromise between enhanced $_iH_c$ and reduced J_r (which reflects a balance between enhanced J_r, associated with exchange coupling and reduced J_r , associated with reduced J_s.

3.3 Co-susbtituted -(Co,Fe)/$RE_2Fe_{14}B$ alloys

Diffractograms for the OA $(Nd_{0.75}Pr_{0.25})_{10}$ $(Fe_{0.9}Co_{0.1})_{80-x}Nb_xB_{10}$ (x = 0, 2, 4) alloy series are shown in Fig.8. For the Nb-free alloy, again, the presence of bcc α-(Fe,Co) phase is manifested as a strong diffraction peak at 2θ= 44.6° together with 2/14/1 phase reflections. For increasing Nb content, the intensity of the α-(Fe,Co) peak exhibits a strong decrease between x = 0 and x = 2, without evident increase in breadth, indicating a reduced α-(Fe,Co) content.

Transmission electron micrographs for two selected OA nanocomposite alloys, $(Nd_{0.75}Pr_{0.25})_{10}$ $(Fe,Co)_{80}B_{10}$ and $(Nd_{0.75}Pr_{0.25})_{10}(Fe,Co)_{78}Nb_2B_{10}$, are shown in Fig. 9. For the Nb-free sample, Fig. 9(a) shows, again, an inhomogeneous structure including very fine crystallites (< 15 nm) distributed among relatively coarse grains (> 50 nm), whilst for the alloy with 2 at% of Nb, Fig. 9 (b), a more homogeneously refined structure (with mean grain size diameter < 40 nm) was promoted by Nb addition.

The second quadrants of the *J-H* loops for this alloy series are shown in Figs. 10 and 11. For the RE=8 at% series (Fig. 10), $_iH_c$ increases progressively as the Nb concentration *x* increases: from 228 kA/m up to 670 kA/m, though with a significant reduction in J_r between 2 and 4 at% Nb (from 1.04 T to 0.94 T). $(BH)_{max}$ is increased significantly on adding Nb from 60 kJ/m^3 up to 129 kJ/m^3, which is largely a reflection of the very low $_iH_c$ for the Nb-free alloy.

For the RE = 10 at% series (Fig. 11), consistently larger $_iH_c$ values were observed, ranging from 619 kA/m up to 919 kA/m, consistent with the smaller volume fraction of soft magnetic phase(s) present, and with $(BH)_{max}$ being as high as 123 kJ/m^3 for the 2 at% Nb alloy.

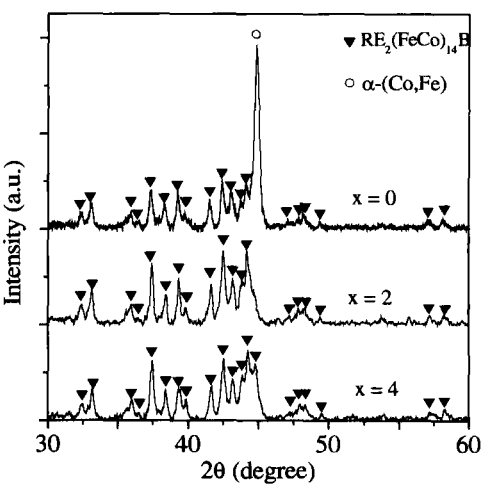

Fig. 8 X-ray diffractograms for OA $(Nd_{0.75}Pr_{0.25})_{10}$ - $(Fe_{0.9}Co_{0.1})_{80-x}Nb_xB_{10}$ (x = 0,2,4) alloy ribbon series

Table 3 summarizes the magnetic property data for this alloy series. Again, as for the Co-free series, Nb causes a sharp reduction in J_s and, for 10 at% RE series in particular (for which volume fraction of soft phase is smaller), this leads to a marked effect on J_r.

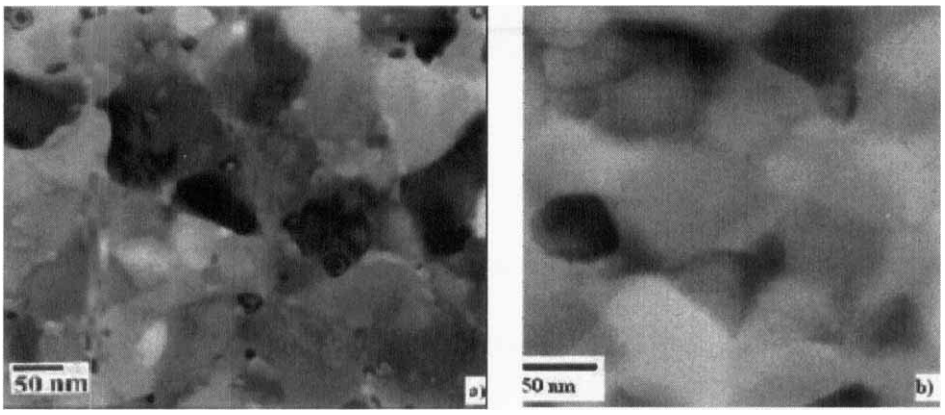

Fig. 9 TEM micrographs for OA $(Nd_{0.75}Pr_{0.25})_{10}(Fe,Co)_{80}B_{10}$ (a) and $(Nd_{0.75}Pr_{0.25})_{10}(Fe,Co)_{78}Nb_2B_{10}$; (b) nanocomposite ribbons

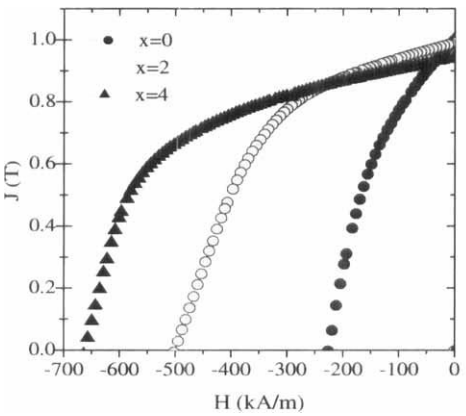

Fig. 10 J-H demagnetising curves for OA $(Nd_{0.75}Pr_{0.25})_8$-$(Fe_{0.9}Co_{0.1})_{82-x}Nb_xB_{10}$ (x = 0,2,4) alloy ribbon series

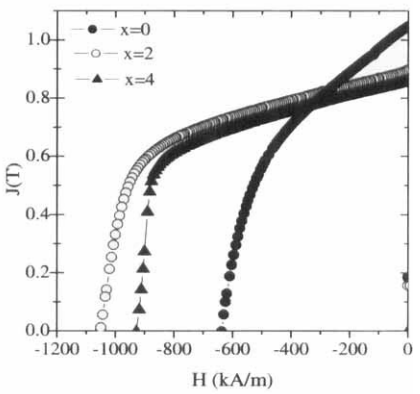

Fig. 11 J-H demagnetising curves for OA $(Nd_{0.75}Pr_{0.25})_{10}$-$(Fe_{0.9}Co_{0.1})_{80-x}Nb_xB_{10}$ (x = 0,2,4) alloy ribbon series

Table 3 Magnetic properties of OA ribbon samples of alloys in system $(Nd_{0.75}Pr_{0.25})_y$-$(Fe_{0.90}Co_{0.1})_{90-y-x}Nb_xB_{10}$

RE content (y); Nb content (x)	$_iH_c$ (kA/m)	J_r (T)	J_s (T)	$(BH)_{max}$ (kJ/m^3)
y=8, x=0	228 ± 10	1.04 ± 0.06	1.75 ± 0.04	60 ± 7
y=8, x=2	501 ± 7	0.97 ± 0.02	1.48 ± 0.02	124 ± 4
y=8, x=4	670 ± 10	0.94 ± 0.01	1.40 ± 0.03	129 ± 4
y=10, x=0	619 ± 24	1.05 ± 0.02	1.60 ± 0.02	128 ± 9
y=10, x=2	1042 ± 15	0.88 ± 0.01	1.37 ± 0.01	123 ± 5
y=10, x=4	919 ± 8	0.84 ± 0.02	1.32 ± 0.04	116 ± 6

4 Conclusions

A remarkable enhancement of $_iH_c$ (up to 1042 kA/m for y=10, x=2 and TM =Fe+Co composition) was observed for overquenched and annealed ribbons in the $RE_yTM_{90-y-x}Nb_xB_{10}$ (RE=Nd, Nd+Pr, TM=Fe, Fe+Co; y=8,10,12, x=0,2,4) alloy series. TEM observations revealed a considerable grain size refining effect promoted by the Nb additions, which is considered to be responsible for the increased $_iH_c$. This $_iH_c$ enhancement, in addition to the improved squareness of the demagnetising curves, resulted in very good maximum energy densities (up to 140 kJ/m^3 for y=10, x=2 and TM = Fe composition) thus rendering this alloy series a promising candidate for bonded magnet applications.

Acknowledgements

I.B. and H.A.D. are grateful to The Royal Society for financial support for I.B.'s visit to the University of Sheffield. I.B. also acknowledges research funding through project IN119603-UNAM and helpful technical assistance from Mr C.Flores.

References:

[1] Coehoorn R, de Mooij D B, Duchateau J P W B, Buschow K H J, J. Physique, 1988, C8: 669.

[2] Kneller E, Hawig R, IEEE Trans. Magn., 1991, 27: 3588.

[3] Manaf A, Buckley R A and Davies H A, J. Magn. Magn. Mater., 1993, 128:302.

[4] Ding J, McCormick P G and Street R, J. Magn. Magn. Mater., 1993, 124: 1.

[5] CHEN Z M, NI C Y and Hadjipanayis G C, J. Magn. Magn. Mater., 1998, 186: 41.

[6] Fischer R, Schrefl R, Kronmuller H and Fidler J, J. Magn. Magn. Mater., 1996, 153: 35.

[7] Davies H A, Proceedings of the 8th Symp. on Magnetic Anisotropy and Coercivity in RE-TM Alloys. Eds. C.A.F. Manwaring et al. University of Birmingham: UK, 1994. 465.

[8] Davies H A, Harland C L , Betancourt J I. and Mendoza G. Proceedings of the MRS Symp. on Advanced Hard and Soft Magnetic Materials. Eds. Michael Coey et al. p 27, Warrendale,: USA, 1999.

[9] Harland C L, Davies H A, J. Appl. Phys., 2000, 87: 6116.

[10] Kojima A, Ogiwara F, Makino A and Inoue A, Masumoto T, Mater. Sci. and Eng., 1997, A226-228: 520.

[11] WANG Z, ZHOU S, ZHANG M, QIAO Y and WANG, J. Appl. Phys., 1999, 86: 7010.

[12] [12] WANG Z, ZHOU S, ZHANG M, QIAO Y, GAO X, ZHAO Q, WANG R and GONG W, J. Appl. Phys., 1999, 85: 4880.

[13] Gabay A M, Popov A G, Gaviko V S, Belozerov Y V and Yermolenko A S, J. Alloys and Comp.,1996, 245: 119.

[14] Betancourt I and Davies H A, J. Magn. Magn. Mater., 2003, 261: 328.

[15] CHEN Z, ZHANG Y, DING Y and Hadjipanayis G C, J. Appl. Phys., 1999, 85: 5908.

[16] LIU J F, Davies H A, J. Magn. Magn. Mater., 1996, 157/158: 29.

[17] LIU Z, Davies H A. Proceedings of the 18th Int. Workshop on High Perform. Magnets and Appl. Ed N.M. Dempsey and P. de Rango pp.715-722 :Annecy, 2004.

[18] CHANG W C, Chiou D Y, Wu S H, Ma B M, Bounds C O, Appl.Phys.Lett.,1998, 72: 121.

[19] CHANG W C, WANG S H, CHANG S J, Tsai M Y, .Ma B M, IEEE Trans. Magn.,1999, 35: 3265.

[20] Hirosawa S, Kanekiyo H, Shigemoto Y, Miyoshi T, Proceedings of the 18th International Workshop on High Performance Magnets and Their Applications, Annecy, France: 2004.

[21] Davies H A , J. Magn.Magn.Mater.,1996, 157/158:11.

[22] YING H, WU C H, CHUANG Y C, J. Less-Common Met., 1987, 132: 317.

[23] Schrefl T, Fischer R, Fidler J and Kronmuller H, J. Appl. Phys,1994, 76: 7053.

[24] Betancourt J I and Davies HA , J. Magn. Magn. Mater., 2002, 246: 6.